Int. J. Environ. Sci. Technol. (2018) 15:105–118
https://doi.org/10.1007/s13762-017-1369-0

ORIGINAL PAPER

Removal of cadmium (II) from aqueous solution and natural water samples using polyurethane foam/organobentonite/iron oxide nanocomposite adsorbent

M. Sayed[1] · N. Burham[1]

Received: 1 September 2016 / Revised: 5 February 2017 / Accepted: 9 May 2017 / Published online: 30 May 2017

Abstract A novel polyurethane foam/organobentonite/iron oxide nanocomposite adsorbent was successfully prepared via in situ polymerization of toluene diisocyanate and polyol in presence of 5 wt% organobentonite/iron oxide. The obtained nanocomposite was characterized in detail, and the results revealed that the clay layers are exfoliated and/or intercalated in the polymer matrix forming a nanocomposite structure. The application of the prepared nanocomposite for adsorption of cadmium ions from aqueous solution was tested as a function of various experimental parameters using batch procedures. Adsorptive removal of Cd(II) onto the nanocomposite attained maximum at adsorbent content 1.5 g/L, pH 6, and the equilibrium was established within 60 min. Kinetic studies showed that the experimental data fit very well to pseudo-second-order model, and the adsorption process proceeds through three steps. It was found that external liquid film and intraparticle diffusion steps deeply affect the rate of Cd^{2+} ions adsorption onto the synthesized nanocomposite. Langmuir isotherm model fitted the adsorption data better than Freundlich with a maximum adsorption capacity (q_m) for Cd(II) equal to 78 mg/g under the specified experimental conditions. The synthesized nanocomposite afforded effective extraction for Cd^{2+} ions from natural water samples and excellent reusability feature. This study declares the potential efficiency of a new clay/polymer nanocomposite as alternative for wastewater remediation.

Keywords Analytical application · Cadmium removal · Kinetics · Nanocomposite · Reusability

Editorial responsibility: Abhishek RoyChowdhury.

✉ N. Burham
n_burham@yahoo.com

[1] Chemistry Department, Faculty of Science, Fayoum University, Fayoum 63514, Egypt

Introduction

Heavy metals pollution increases with the rapid development of industries such as metal plating, mining operations, paper, fertilizers, tanneries, batteries and pesticides (Hebbar et al. 2016). Unlike other water contaminants, heavy metals are not biodegradable and tend to accumulate in living organisms causing ecological disturbances and serious threat to human health (Dong et al. 2015). Cadmium is one of the most toxic heavy metals due to its carcinogenic potency even at very low level of exposure (Galbeiro et al. 2014). Long-term exposure to cadmium can also produce serious damage to kidneys, liver and bones (Bailey et al. 1999). The World Health Organization (WHO) and the Environmental Protection Agency (EPA) recommend a 0.003 mg/L standard for Cd(II) in drinking water (Khairy et al. 2014). Therefore, cadmium ions removal from wastewater before discharging into the environment is a crucial process that attracts a great deal of attention (Galbeiro et al. 2014; Khairy et al. 2014; Chen et al. 2011).

Various methods and techniques have been studied and applied for Cd(II) removal including adsorption (Chen et al. 2011; Oliveira et al. 2003), precipitation (Lin et al. 2005), ion exchange (Kocaoba 2007) and electrodialysis (Marder et al. 2004). Most of these processes have its own limitations in terms of incomplete extraction, production of secondary wastes or high operation cost/energy consumption. In this view, adsorption is considered a superior technique due to its extraction effectiveness even at

ultratrace amounts, easy handling, low operation cost, availability of different adsorbents and possibility of adsorbents reusability using a suitable desorption process (Mahmud et al. 2016). A large number of adsorbents have been studied for Cd(II) extraction from wastewater including natural or synthetic zeolites and clay minerals, activated carbon, functionalized polymers, metal oxides, graphene oxide, metal-organic frameworks and carbon nanotubes. Due to their natural abundance, high specific surface area and cation exchange capacity and chemical/mechanical stability, clay minerals are widely used for cadmium ions removal from wastewater (Burham and Sayed 2016). Bentonite is a 2:1 phyllosilicate mineral consisting essentially of montmorillonite and characterized by its high cation exchange capacity (CEC = 0.8–1.2 meq/g), large specific surface area and net negative surface charge. These excellent characteristics give bentonite a great potential as a heavy metal ions cleaner (Karapinar and Donat 2009). However, the recovery of bentonite from aqueous media after the adsorption process is very difficult due to its small particle size and high hydrophilic property where it can swell up to 30-fold its original volume forming a very stable colloidal suspension in water. These restrict the practical application of bentonite as extractor (Wang et al. 2014). This problem can be overcome by using bentonite as a filler with various polymer matrices to prepare clay/polymer nanocomposites (CPNs) where the clay platelets are intercalated and/or exfoliated by the polymer chains.

CPNs are a new category of adsorbents that formed when small amount (typically less than 10 wt%) of a clay mineral is dispersed in a polymer matrix (Bergaya and Lagaly 2007). They characterized by improved chemical and mechanical stability and excellent adsorption efficiency. In the present work, a novel magnetic polyurethane foam/organobentonite/iron oxide (PUF/OB/IO) nanocomposite was prepared via in situ polymerization of toluene diisocyanate (TDI) and polyol in presence of organobentonite coated with iron oxide particles. Organobentonite was prepared through exchanging the interlayer cations with hexadecyltrimethylammonium bromide (HDTMAB) to boost the nanocomposite formation. Polyurethane foam has been chosen as the polymer matrix based on its high available surface area, cellular structure and extremely low cost. In addition, it is stable in acids, bases and organic solvents (Azeem et al. 2010). The synthesized material was characterized in detail to investigate its physical and chemical properties. The applicability of the obtained nanocomposite for extraction of Cd(II) from aqueous solution was tested using the batch technique. The overall performance of PUF/OB/IO nanocomposite adsorbent was estimated in terms of sorption isotherms, kinetics and effects of various parameters (pH, uptake time, sorbent dose and initial metal ion concentration). Considering the practical application of the prepared PUF/OB/IO nanocomposite, the regeneration and analytical applicability for real samples were also examined. The prepared nanocomposite adsorbents showed considerable improved features compared to the bare clay in terms of higher adsorption capacity, extremely ease of separation and excellent reusability aspects. It is worth to mention that this work was done during the summer of 2016 at the inorganic chemistry laboratory, Faculty of Science, Fayoum University, Egypt.

Materials and methods

Materials

The raw bentonitic clay was collected from Qalamshah–Fayoum–Egypt, where excessive bentonite deposits are existent with thickness of 2–3 m (Agha et al. 2015). The raw clay was purified according to the procedure described in the literature (Shah et al. 2013); the purified clay was sodium exchanged using 3 wt% anhydrous sodium carbonate and denoted Na–B. The cation exchange capacity (CEC) and specific surface area (SSA) of Na–B sample were found to be 85 meq/100 g and 367 m^2/g using methylene blue spot and titration methods (Yukselen and Kaya 2008), respectively.

HDTMAB (Merck, Germany), polyol and TDI (Adwic, El-Nasr, Egypt) are of analytical grade and used without further purification. A stock solution of cadmium (1000 ppm) was prepared by dissolving appropriate amount of $Cd(NO_3)_2{\cdot}4H_2O$ (Panreac, Barcelona, Spain) in double distilled water (DDW) then acidified by 2 mL HNO_3 acid. Working solutions were daily prepared from the stock by appropriate dilution; the pH of the solutions is adjusted by controlled addition of HCl or NaOH.

Preparation of the magnetic nanocomposite adsorbent

Preparation of iron oxide (IO)

Iron oxide was prepared using a slightly modified procedure (Cottet et al. 2014): Ammonia solution (2.0 mol/L) was slowly added to a 100 mL solution containing $FeCl_3$ (2.0 mol/L) and $FeSO_4$ (1.0 mol/L) under mechanical stirring at 500 rpm until the pH of the solution reach between 11 and 12. The product was washed several times with DDW until the pH became 7 then oven-dried at 80 °C for 8 h, grinded, passed through 140 μm sieve and stored in a desiccator for further use.

Preparation of organobentonite/iron oxide (OB/IO)

Organobentonite/iron oxide was prepared by simultaneous intercalation of both HDTMAB and IO as follow: 5 g of Na–B was added in portions to 85 mL DDW at 70 °C under magnetic stirring until thoroughly dispersed. HDTMAB (3.076 g, equivalent to 2 CEC of the Na–B sample) and IO (2.5 g) were mixed in 85 mL DDW at 70 °C; then, this mixture was added to the bentonite suspension under mechanical stirring at 1000 rpm for 1 h at 70 °C. The product was aged for 4 h, vacuum-filtered, washed several times with DDW until free from bromide ion (testing with 0.1 N $AgNO_3$), oven-dried at 60 °C for 12 h then grinded, passed through 140 μm sieve and stored in a desiccator for further use.

Preparation of polyurethane foam/organobentonite/iron oxide (PUF/OB/IO)

The hybrid material was prepared through a two-step process where: 1.9 g OB/IO (represent 5 wt%) was dispersed in 20 g polyol followed by addition of 2 drops of stannous octoate with vigorous stirring. To this dispersion, a mixture containing 13.5 g TDI, 2 drops of silicon oil and 2 mL distilled water were gradually added with continuous stirring. During foaming, the liquid polymer was poured into a mold and left for 24 h at room temperature. The foam material was cut into small cubes (0.2 cm in dimension) rinsed overnight in distilled water, washed with 0.1 M HCl to remove excess inorganics, washed with acetone to remove excess organics and finally washed with distilled water and then air-dried.

Characterization

Various characterization techniques were employed to investigate the physiochemical properties of bare bentonite, organo-inorganobentonite and the nanocomposite. The phase identification and X-ray diffraction (XRD) pattern of the samples were analyzed using PANalytical X-ray diffractometer model X'Pert PRO (Netherlands). Fourier transform infrared (FTIR) spectra of the samples were recorded in the range of 4000–400 cm^{-1} using Mattson Satellite FTIR spectrometer model 2000 (Madison, USA). The solid samples were pulverized and mixed together with KBr powder with 1/100 w/w ratio, pressed into pellets for 2 min at 120,000 psi. The morphology and elemental composition of each sample were analyzed using a field emission scanning electron microscope (SEM; Quanta 250 FEG, FEI company, Netherlands) attached with energy-dispersed X-ray spectroscopy (EDS) unit. All samples were coated with gold before SEM analysis. Transmission electron microscopy (TEM) micrograph of PUF/OB/IO nanocomposite was obtained from a JEM-HR-2100 (Japan).

Adsorption experiments

The adsorption experiments were performed using batch equilibrium technique at ambient temperature. All the adsorption experiments were carried out using 25 mL cadmium ion working solution in 250-mL polyethylene bottles. Different experimental parameters affecting the removal process were studied including pH, adsorbent dosage, contact time and initial metal ion concentration. The pH was measured using the microprocessor pH meter BT 500 (Boeco, Germany) and adjusted by adding HCl or NaOH. The adsorption kinetics was studied by varying the uptake time over the interval 2–90 min using orbital shaker at a speed of 200 rpm. Also, the adsorption isotherm was evaluated by varying the initial metal ion concentration over 0.6–100 ppm. All the experiments were conducted for three times, and the average values are reported. Error bars representing the standard deviation from the mean value are also introduced to each plot of the adsorption experiments. Residual Cd(II) ion concentrations were measured using atomic absorption spectrophotometer (Shimadzu, AA-7000). The amount of Cd(II) adsorbed can be derived from the initial (C_o) and the equilibrium ($C_{eq.}$) cadmium ion concentrations:

$$q_e = \frac{(C_o - C_{eq})V}{m} \quad (1)$$

where q_e (mg/g) is the amount of Cd(II) adsorbed, C_o (mg/L) is the initial Cd(II) concentration, C_{eq} (mg/L) is the equilibrium concentration of Cd(II) after the adsorption process, m (g) is the mass of the adsorbent and V (L) is the volume of the Cd(II) solution. The % removal of Cd(II) by the PUF/OB/IO nanocomposite is calculated from the difference between initial and final Cd(II) concentrations according to Eq. 2:

$$\%\text{Removal} = \frac{(C_o - C_{eq})}{C_o} \times 100 \quad (2)$$

Regeneration and desorption studies

The regeneration experiments were conducted to estimate the reusability of the PUF/OB/IO nanocomposite adsorbent and discover the efficient reagent for effective Cd(II) desorption from the nanocomposite. For this purpose, 0.05 g from the nanocomposite was mixed together with 100 ppm Cd(II) solution at pH 6 and agitation speed 200 rpm for 1 h. After that, the loaded samples were washed with DDW and air-dried. Secondly, each sample was treated with a different eluting reagent (HCL, HNO_3 or H_2SO_4) at the same volume and concentration (25 mL and 0.1 M,

respectively). The concentration and volume impact—of the eluting agent—on the desorption process was also tested. After each desorption experiment, the adsorbent samples were washed several times with DDW till free from acid, air-dried and used for the next run. The reusability of the PUF/OB/IO nanocomposite for Cd(II) adsorption was assessed by repeating six cycles of successive adsorption and desorption.

Application for real samples

To ensure the practical application of the synthesized nanocomposite adsorbent, two real samples, Qaroun Lake water and regional Nile river water, were collected and treated by PUF/OB/IO nanocomposite using batch procedure. Firstly, the water samples were filtered using Whatman filter paper No. 42 to remove suspended particulates. Then, 1 L from each sample was placed in a clean glass bottle and spiked with 0, 50 or 200 µg from Cd^{2+}. Afterwards, each sample was mixed with 0.1 g PUF/OB/IO for 1 h by the orbital shaker at 200 rpm. Finally, the Cd-laden PUF/OB/IO samples were separated from the water samples, eluted by 25 mL 1 M nitric acid and the concentration of Cd^{2+} eluted was determined by ICP-OES.

Results and discussion

Characterization

X-ray diffraction (XRD)

The XRD patterns of Na–B, OB/IO and PUF/OB/IO samples are presented in Fig. 1a–c, respectively. The wide reflection between $2\theta = 5°$ and 20° is attributed to interstratified clay minerals, mainly montmorillonite and kaolinite (Kurko and Matović 2015) (Fig. 1a). The two peaks at $2\theta = 20.1°$ and 26.43° are characteristic for quartz as a non-clay component, even after purification. The 001 reflection corresponding to Na–B sample at $2\theta = 7.9°$ (d-spacing = 11.19 Å) indicates that the bentonite sample is in the sodium form (Jovic-Jovicic et al. 2008) which asserts the activation step. The shift of the 001 reflection from 2θ 7.9° to 4.4°(d-spacing = 20.06 Å) in OB/IO pattern suggests intercalation of $HDTMA^+$ ions within the interlayer structure. From the d-spacing value (2.006 nm), it can be proposed that the arrangement of the $HDTMA^+$ ions within the interlayer spaces is a pseudo-trilayer configuration. Since the thickness of phyllosilicate's TOT layer is 0.96 nm, a 1.046-nm interlayer space indicates the presence of a bilayer mirror image arrangement of $HDTMA^+$ ions (Zhu et al. 2003) as depicted in Fig. 2. The peak at $2\theta = 35.5°$ in the patterns of OB/IO and PUF/OB/IO is a characteristic band for iron oxide which implies that IO particles may be grafted to the bentonite surface. The absence of the typical 001 diffraction peak in the PUF/OB/IO pattern suggests that OB was exfoliated and dispersed in the PUF matrix forming nanocomposite structure (Wu et al. 2013). Moreover, the broad hump at $2\theta = 20°$ is due to the bulk polyurethane polymer portion of the sample (Khudyakov et al. 2009).

FTIR analysis

FTIR spectra of Na–B, OB/IO and PUF/OB/IO are depicted in Fig. 3. The absorption band at 632 cm^{-1} in OB/IO patterns is assigned to Fe–O vibration (Cottet et al. 2014); this bands is blue shifted to 662 cm^{-1} in the nanocomposite spectrum indicating an interaction between Fe–O surface groups and PUF matrix. This interaction is very

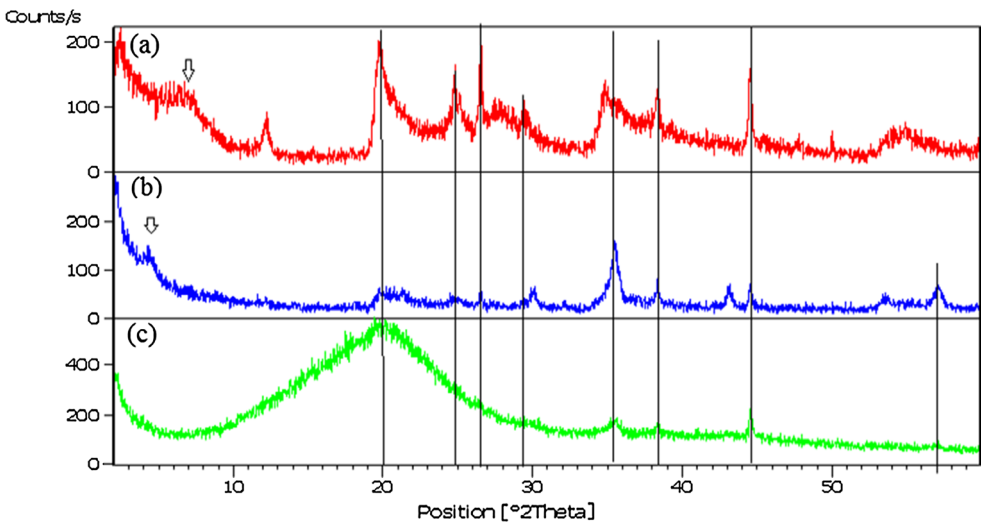

Fig. 1 X-ray diffraction patterns of **a** Na–B, **b** OB/IO and **c** PUF/OB/IO

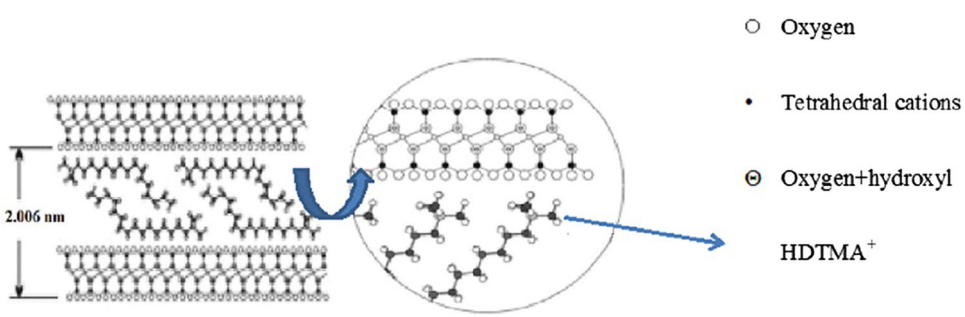

Fig. 2 Schematic representation of pseudo-trilayer arrangement of $HDTMA^+$ ions within the interlayer space (Zhu et al. 2003)

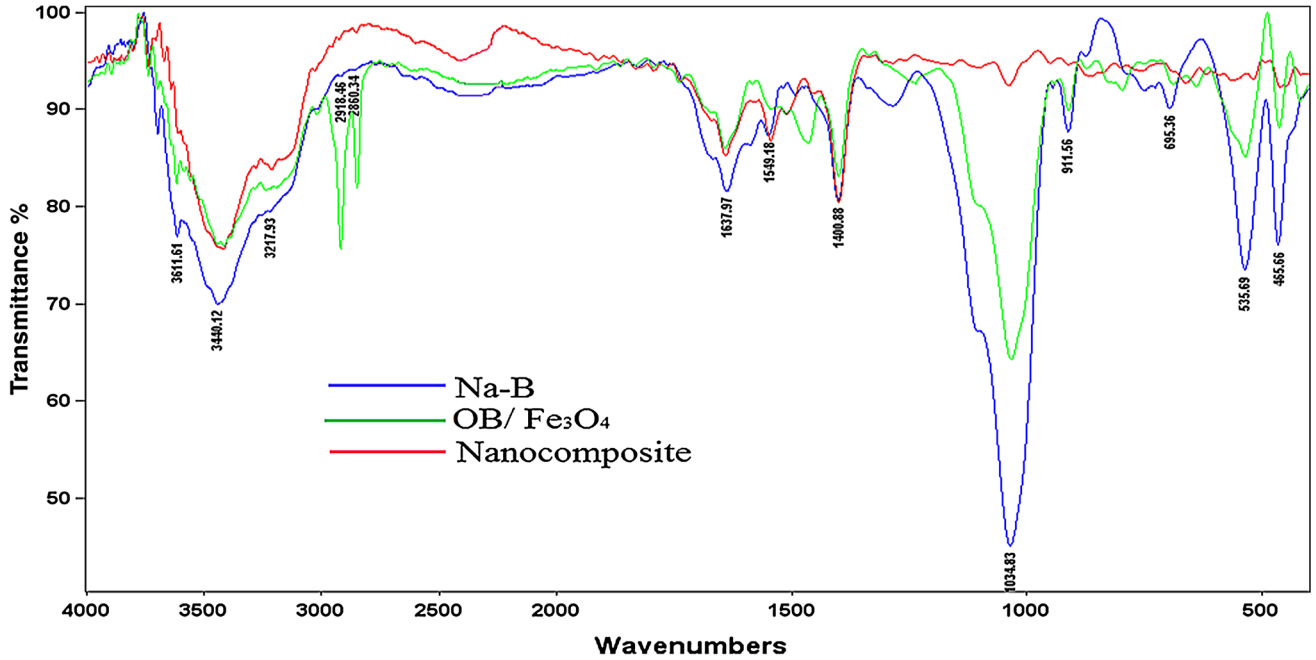

Fig. 3 FTIR spectra of Na–B, OB/IO and PUF/OB/IO

important for the stability of the prepared nanocomposite (LUO et al. 2016).The peaks at 911, 1034 and 1400 cm^{-1} were tentatively assigned to Al–O and Si–O stretching and C–H bending modes, respectively (Wu et al. 2013). The appearance of three new peaks in the OB/IO chart at 2918, 2860 and 1474 cm^{-1} agree well with asymmetric and symmetric stretching and bending vibration of $–CH_2$ group in the surfactant chain. In addition, the two bands at 3440 and 1638 cm^{-1} are attributed to O–H stretching and bending, respectively. The peaks at 1850, 1539, 1303 and 1100 cm^{-1} and that around 3272 cm^{-1} in the nanocomposite chart are due to aromatic C–H, aromatic C = C, C–N, –CO and –NH, respectively. The decrease in the band intensity appearing at 3611 cm^{-1} (which assigned to free hydroxyl groups) in PUF/OB/IO pattern compared to Na–B and OB/IO patterns strongly recommends that PUF reacted with –OH groups on the surface of OB/IO resulting in a decreased number of free –OH groups. This interaction is also substantial to produce stable polyurethane nanocomposite (Zhou et al. 2010). Presence of diverse functionality (aluminol, silanol, free hydroxyl, carbonyl and amino groups) within the stable structure of the synthesized nanocomposite greatly supports its practical application as adsorbent in the wastewater treatment field.

SEM–EDS analysis

SEM images coupled with the corresponding EDS analyses for Na–B, OB/IO and PUF/OB/IO samples are presented in Fig. 4a–c. The perfect layer to edge sheet-like structure of bentonite is obvious in Fig. 4a; the corresponding EDS analysis indicates that the main elemental components of bentonite are silicon, aluminum and oxygen in the form of aluminosilicates. Organo-modification largely changes the texture of bentonite where the surface seems to be covered with organic moieties as a result of intercalation by $HDTMA^+$ ions (Fig. 4b1). Accordingly, the EDS result displays the disappearance of sodium ion peak along with increasing the carbon content as a powerful evidence for the intercalation process. Figure 4b2 shows lighter entities

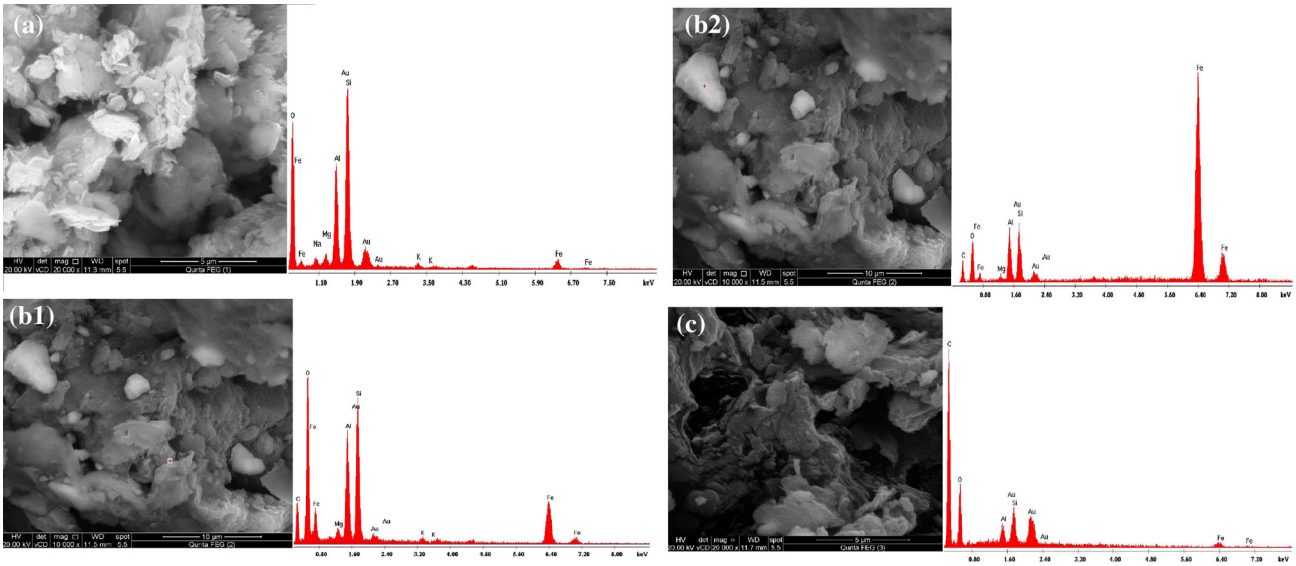

Fig. 4 SEM–EDS of **a** Na–B **b1** OB/IO **b2** OB/IO with different spot for EDS **c** PUF/OB/IO

which represent aggregates of iron oxide particles as confirmed by the EDS analysis indicating that iron oxide particles could be grafted on the surface and/or intercalated onto the gallery. Edge curling dispersed clay layers inside the cellular structure of polyurethane foam (Fig. 4c) confirming clay exfoliation (Block et al. 2015). The corresponding EDS analysis declares the elemental composition of a typical CPN with major % composition for the polymer matrix represented in carbon and minimal % composition for the inorganic clay filler.

TEM analysis

TEM micrograph of the PUF/OB/IO nanocomposite is shown in Fig. 5. Dispersion of organobentonite platelets (encircled darker lines) in the PUF matrix assures the exfoliation and/or intercalation of the clay platelets and formation of nanocomposite structure as argued from the results of XRD and SEM analyses. Intense dark spots in the micrograph are attributed to iron oxide particles.

Adsorption experiments

Effect of pH

Solution pH is the most important parameter affecting heavy metals removal from aqueous media as it not only influences the metal ion speciation but also the charges on the active extraction sites (Zhao et al. 2010). For this purpose, the effect of solution pH on the removal of Cd(II) from aqueous solution onto PUF/OB/IO nanocomposite was studied over the pH range 3–9 and the results are plotted in Fig. 6a. The uptake efficiency increases from 73 to 98% as the pH increases from 3 to 6 and maintains a high level. At lower pH values, there is a competition between hydrogen and cadmium ions towards adsorption

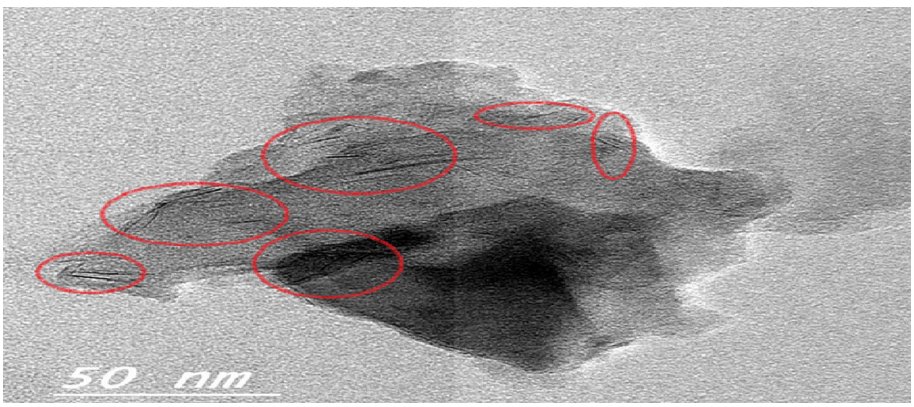

Fig. 5 TEM image of PUF/OB/IO nanocomposite

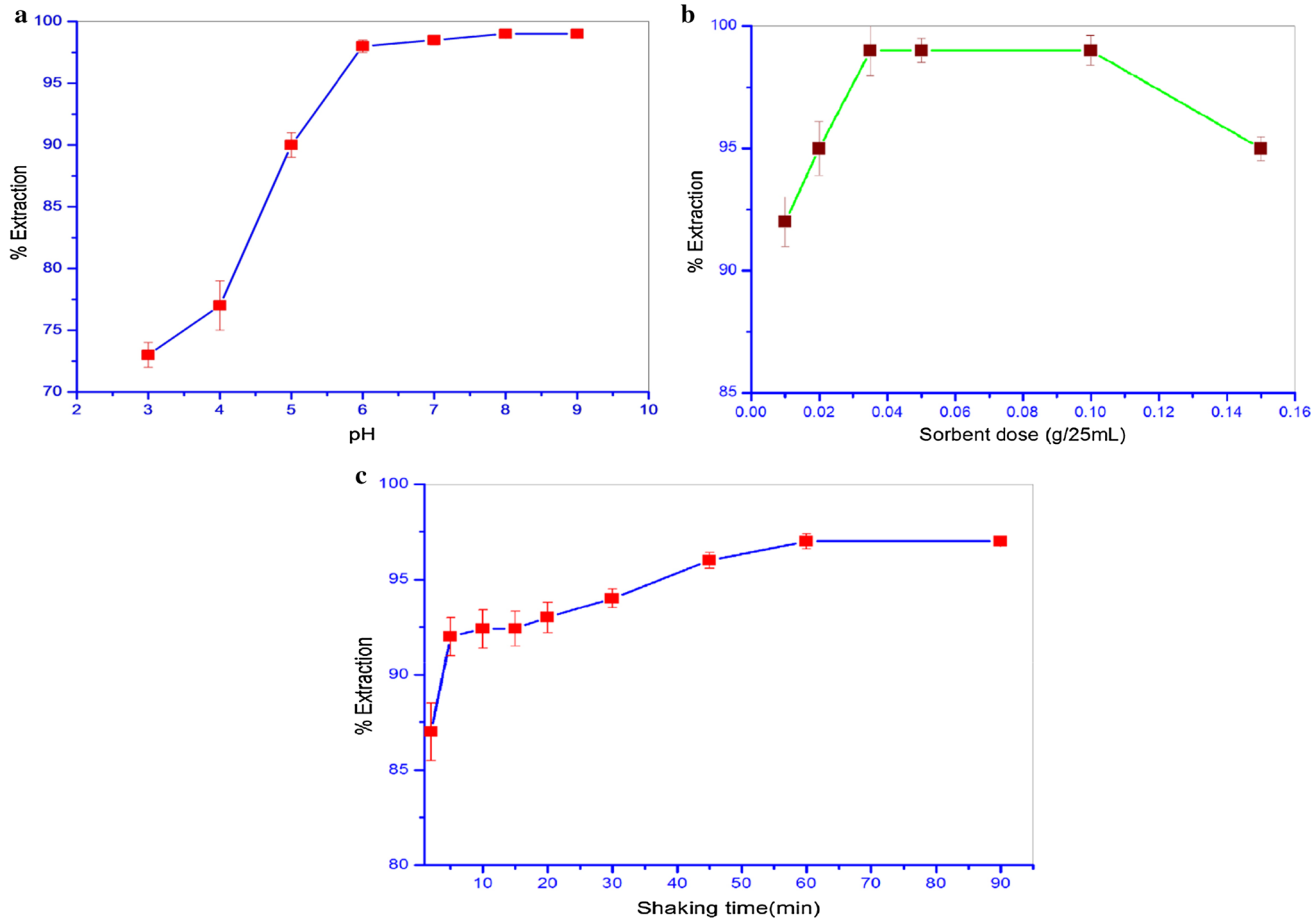

Fig. 6 Effect of **a** pH, **b** sorbent dose and **c** shaking time on the extraction of Cd(II) onto PUF/OB/IO nanocomposite at $C_o = 0.8$ ppm

onto the nanocomposite binding sites. Also, the protonation of the surface functional groups impedes the adsorption of Cd(II) due to electrostatic repulsion (Cottet et al. 2014) which decline the uptake %. With pH rising, the removal efficiency enhanced as the competition between H^+ and Cd^{2+} gets minimized and the surface functional groups acquire negative charges due to deprotonation. These changes promote (1) surface adsorption, (2) surface complexation and (3) electrostatic attraction of the metal ion under consideration towards the adsorbent (Wu et al. 2013). Beyond pH 8, precipitation of cadmium hydroxide will be a predominant mechanism for Cd(II) removal. As a consequence of the above considerations and negligibility of iron leaching around neutral pH range (Ma et al. 2016; Atia et al. 2005), pH 6 was chosen as optimal pH for further tests.

Effect of adsorbent dosage

Many researchers showed that the adsorbent dosage has a significant effect on the removal of metal ions from aqueous solutions (Setshedi et al. 2013; Zhao et al. 2010). The effect of the nanocomposite content on the extraction of Cd(II) from aqueous solutions was tested over the range 0.01–0.15 g/25 mL, and the results are presented in Fig. 6b. The uptake efficiency enhances with the sorbent content reaching 99% at 0.035 g/25 mL. This could be illustrated in terms of increasing adsorbent content increases the number of active sites available for adsorption and hence efficient extraction was achieved. Above 0.1 g/25 mL dose, the decline of % extraction may be attributed to active sites blocking and/or partial aggregation of the nanocomposite. So we choose 0.035 g/25 mL as the optimum nanocomposite dose for Cd(II) extraction from aqueous solution.

Effect of uptake time

The amount of metal ions retained on the adsorbent surface largely varies with time; therefore, the extraction of cadmium ion from aqueous solution by the nanocomposite was studied over the time interval 2–90 min and the results are depicted in Fig. 6c. As shown in this figure, the extraction efficiency increases rapidly with the contact time where it reaches 94% within 30 min and then increases slowly with longer times, and equilibrium is attained within 60 min.

Therefore, 60-min contact time was chosen as sufficient time to attain equilibrium for Cd(II) ions with the nanocomposite adsorbent. This results indicate that adsorption of cadmium ion onto nanocomposite is a multistage process as will be discussed in the next section.

Adsorption kinetics

To investigate the mechanism of the adsorption particularly the rate-limiting step, the kinetic data were simulated using pseudo-first-order, pseudo-second-order, film diffusion and intraparticle diffusion kinetic models. For pseudo-first-order model which is expressed by Lagergren equation:

$$\ln(q_e - q_t) = \ln q_e - k_1 t \quad (3)$$

where q_e and q_t represent the amount of Cd(II) ion adsorbed (mg/g) at equilibrium and at time t and K_1 (min^{-1}) is the first-order rate constant. A plot of ln (q_e–q_t) *versus* t gives a straight line which allows calculation of the rate constant (k_1) and the equilibrium adsorption capacity (q_e). The convergence of the experimental kinetic data to pseudo-first-order model is presented in Fig. 7a. The corresponding kinetic parameters are shown in Table 1. A very small estimated q_e value compared to the experimental one and a relatively weak fitting to the simulated curve compared with that of pseudo-second-order implying that pseudo-first-order model cannot correlate the experimental kinetic data very well.

The adsorption kinetic data were then analyzed using pseudo-second-order kinetic model which expressed as follows:

$$\frac{t}{q_t} = \frac{1}{2k_2 q_e^2} + \frac{t}{q_e} \quad (4)$$

where k_2 (g/mg min) is the second-order rate constant. The values of the second-order rate constant (k_2) and equilibrium adsorption capacity (q_e) can be calculated from the intercept and slope of a plot between t/q_t and time t.

The kinetic plot of t/q_t versus time t is depicted in Fig. 7b, while the kinetic parameters are given in Table 1. It is clear that pseudo-second-order model describes the adsorption process much better than pseudo-first-order model as the simulated curve better fits to the experimental data and the calculated q_e value is very close to the experimental one (0.571 mg/g). This result emphasizes that adsorption of cadmium ions onto the nanocomposite is due to chemisorption (Ranđelović et al. 2014).

To investigate the rate-determining step that controls the adsorption process, the experimental kinetic data were analyzed using intraparticle and film diffusion models where one or both steps should be involved in the rate-determining step (Qiu et al. 2009).

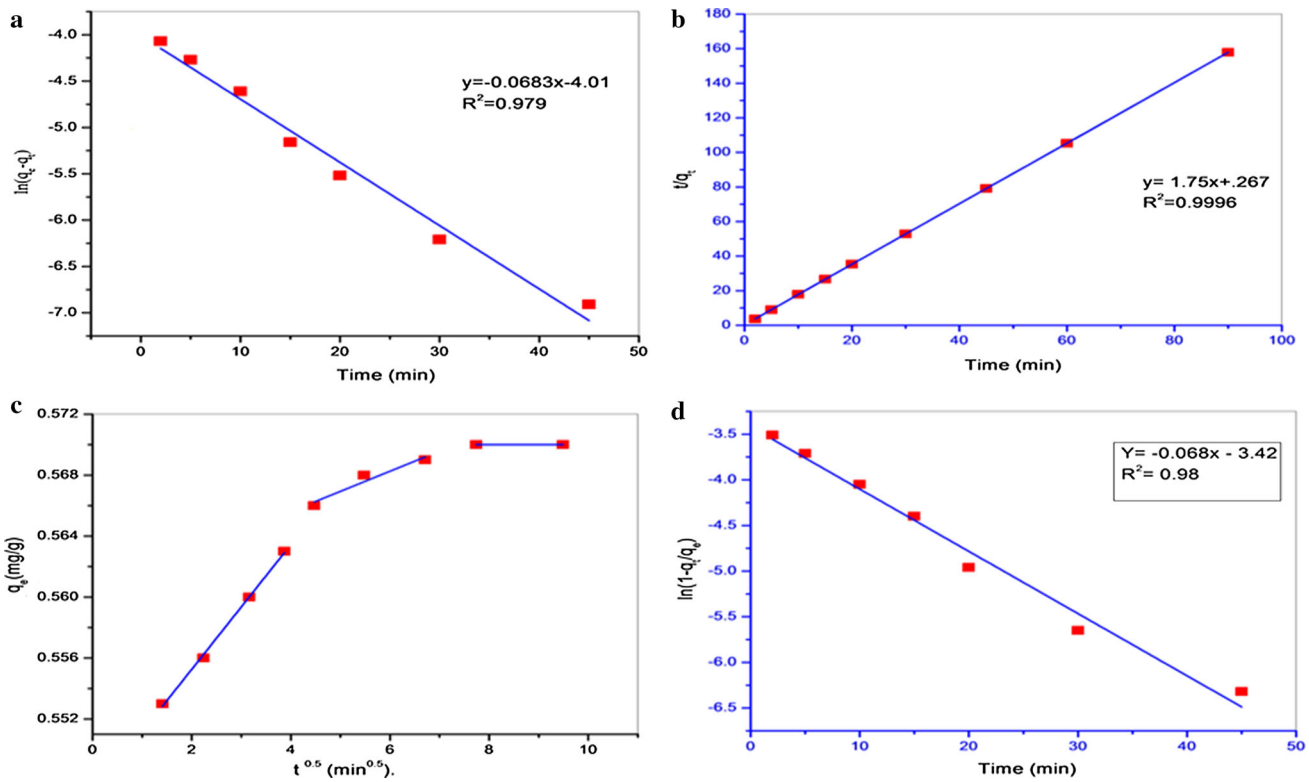

Fig. 7 Fitting of cadmium ion adsorption data onto PUF/OB/IO nanocomposite to **a** pseudo-first-order, **b** pseudo-second-order, **c** Intraparticle diffusion and **d** film diffusion kinetic models

Table 1 Kinetic parameter for pseudo-first-order, pseudo-second-order and film diffusion models

Model	Rate constant	$q_{e\ calc}$(mg/g)	R^2
Pseudo-first-order	$K_1 = 0.068\ min^{-1}$	0.018	0.970
Pseudo-second-order	$K_2 = 11.4$ g/mg min	0.570	0.999
Film diffusion	$R^l = 0.068\ min^{-1}$		0.980

For intraparticle diffusion model, it could be described by Webber–Morris equation:

$$q_t = k_{int} t^{0.5} \tag{5}$$

where k_{int} is the intraparticle diffusion model constant. A plot of q_t versus $\sqrt{t}$ should be a straight line if the intraparticle diffusion is the only rate controlling step. Figure 7c shows a diverse situation, where the plot is nonlinear over all the time range. Instead, the curve can be separated into three linear parts where none of them pass through the origin suggesting that the intraparticle diffusion step is not the only rate-limiting step, but there are three independent steps controlling the adsorption process. This in turn agrees with the results recently reported for adsorption of Cd(II) onto modified magnetic polyacrylamide microcomposite (Zhao et al. 2014).

To ensure that liquid film diffusion step is involved in the adsorption kinetics, the experimental data were fitted according to film diffusion model which is described by the mass transfer rate equation:

$$\ln\left(1 - \frac{q_t}{q_e}\right) = -R^l t \tag{6}$$

where R^l (min^{-1}) is the liquid film diffusion constant. As the model proposed, a straight line plot of $\ln(1 - \frac{q_t}{q_e})$ versus t indicates that liquid film diffusion is involved in the rate-determining step (Qiu et al. 2009). Figure 7d indicates that the external liquid film diffusion step strongly affects the adsorption of Cd(II) onto the PUF/OB/IO nanocomposite where the kinetic data are fitted very well to this model ($R^2 = 0.98$).

Based on these combined evidences, it can be concluded that the process of cadmium ions adsorption onto PUF/OB/IO nanocomposite proceeded via three steps, firstly, rapid external liquid film diffusion then relatively slow pore diffusion and finally adsorption of the ions to the interior binding sites, i.e, bounding pores and capillary spaces.

Adsorption mechanism

It was argued in the previous sections that the process of Cd^{2+} adsorption onto PUF/OB/IO nanocomposite is a chemical in nature. To investigate the type of this chemical binding, the infrared spectra of the nanocomposite before and after the adsorption process were compared as depicted in Fig. 8. The broadband around 3200 cm^{-1} which assigned to –NH groups in the polymer chains was collapsed and blue shifted after adsorption suggesting that the amino groups involved in the adsorption process through complexation with cadmium ions. Bit sharpening of the band at 1670 cm^{-1} which assigned to amide C=O groups after adsorption confirms that cadmium ions were coordinated strongly to them (Zhao et al. 2014). Also, the change in the shape of the bands assigned to silanol (1038 cm^{-1}), aluminol (460 cm^{-1}) and Fe–O (662 cm^{-1}) groups is due to electrostatic attraction and/or ion exchange between these groups and cadmium ions. From these findings, we can conclude that the adsorption process of M(II) onto the nanocomposite proceeded via complexation, electrostatic attraction and/or ion exchange which strongly confirm the previous discussion which also in agreement with previous studies (Liu et al. 2015; Wu et al. 2015).

Adsorption isotherm

The adsorption isotherms are generally used for simulating the experimental data, describing the interaction between adsorbent and adsorbates thus optimizing the adsorption process and allowing the evaluation of the adsorptive capacities of adsorbents. Langmuir and Freundlich isotherms (Eqs. 7 and 8, respectively) are frequently used to evaluate the adsorption behavior of systems under study (Foo and Hameed 2010).

$$q_e = \frac{QbC_e}{1 + bC_e} \tag{7}$$

where q_e, Q and b are equilibrium adsorption capacity (mg/g), maximum monolayer capacity (mg/g) and enthalpy of adsorption (L/mg), respectively.

$$q_e = K_F + C_e^{1/n} \tag{8}$$

where k_F is the unit capacity coefficient and $1/n$ is the Freundlich constant related to the system heterogeneity.

The experimental data were simulated using these models as presented in Fig. 9, and the relative parameters calculated from the two models are listed in Table 2.

As clearly shown, the experimental data are best fitted to Langmuir model which is confirmed by the higher determination coefficient ($R^2 = 0.993$) and the convergence between the estimated q_m value and experimental one. This result suggests that cadmium ions adsorption onto the PUF/OB/IO nanocomposite is a monolayer coverage which agrees with that reported in the literature (Machida et al. 2012; Wu et al. 2015). The separation factor R_L is a characteristic of Langmuir isotherm that can be calculated according to Eq. 9.

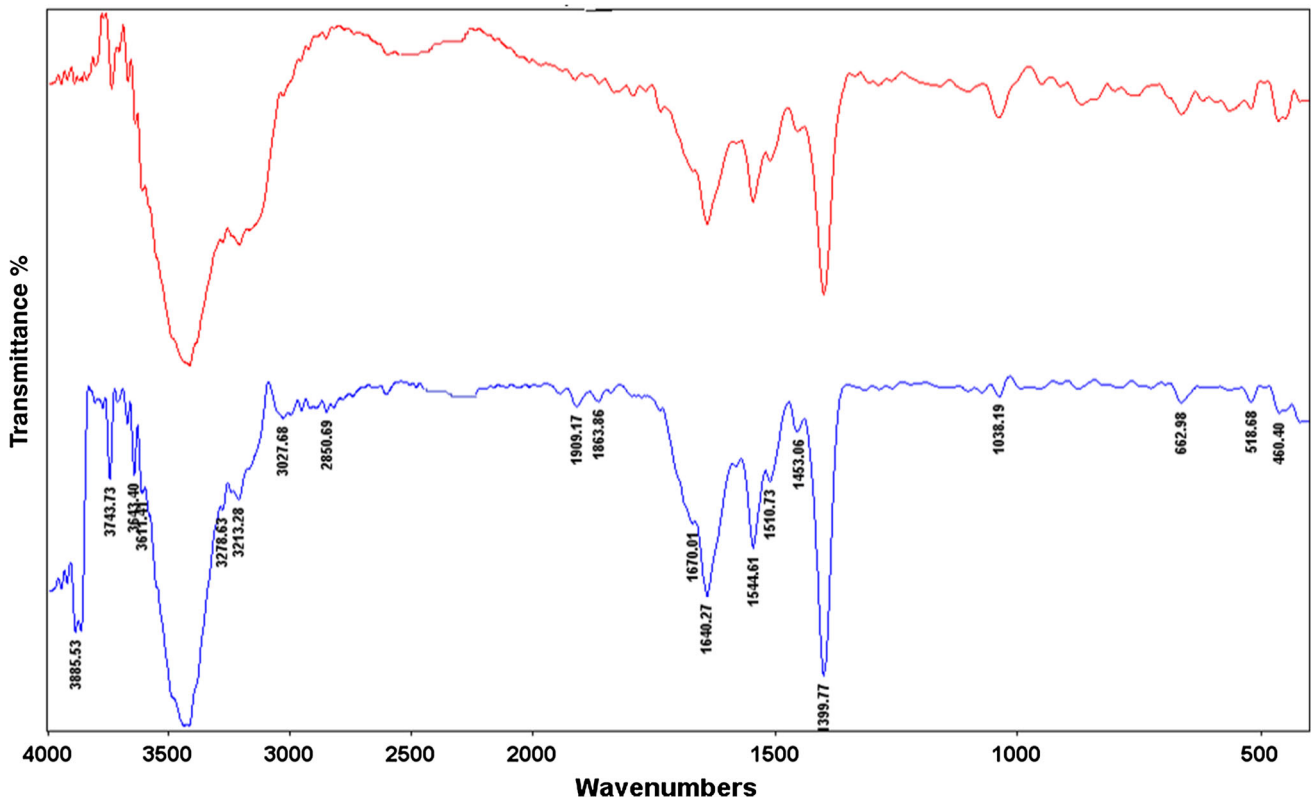

Fig. 8 FTIR spectra of PUF/OB/IO before adsorption (in *red*) and after adsorption (in *blue*)

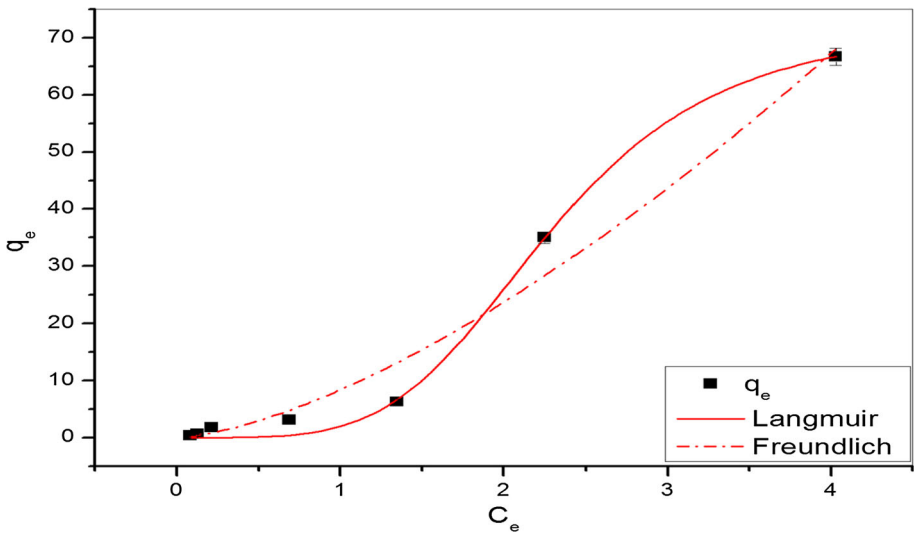

Fig. 9 Nonlinear fit of the experimental adsorption data using Langmuir and Freundlich isotherm models

Table 2 Isotherms parameters for Langmuir and Freundlich models

Langmuir			Freundlich		
Parameter		Standard error	Parameter		Standard error
q_m (mg/g)	72.5	3.6	n	0.66	0.2
K_L (L/mg)	0.03	0.01	K_F (L/mg)	8.37	2.2
R^2	0.993		R^2	0.960	
R_L	0.144–0.960				

$$R_L = \frac{1}{1 + K_L \times C_o} \quad (9)$$

where C_o is the initial solute concentration (mg/L) and K_L is the Langmuir adsorption constant (L/mg). The values of R_L calculated based on Eq. 9 are 0.144–0.96.

From the R_L values and affinity constant 1/n (0.99), it can be concluded that the adsorption of Cd(II) onto the nanocomposite is favorable and the chemisorption process is the predominant mechanism for such adsorption (Foo and Hameed 2010) as confirmed in the previous sections. The maximum adsorption capacity value q_m of PUF/OB/IO nanocomposite for Cd(II) estimated from Langmuir model is 78 mg/g under the given experimental conditions. This value is comparable with that reported using other adsorbents as shown in Table 3. Taking into account the features of simple preparation, facile separation and most importantly costs considerations, PUF/OB/IO nanocomposite can be considered as a promising adsorbent for Cd(II) removal from aqueous solutions.

Desorption and reusability of PUF/OB/IO nanocomposite

The desorption characteristic of PUF/OB/IO nanocomposite was tested using various acidic solutions to find the proper eluting agent for Cd^{2+} (Table 4). Cadmium ions desorption from PUF/OB/IO nanocomposite significantly depends on the composition of the eluting solution. Highest desorption % was noticed for nitric acid where quantitative desorption was achieved by using 1 M nitric acid and no significant increase was observed by raising the concentration. Such findings strongly demonstrates the strong interaction between cadmium ions and the active sites within the nanocomposite. As deduced from the IR spectrum of the nanocomposite after adsorption process, surface complexation and ion exchange are the most probable mechanisms for such strong bonding which reflects the effectiveness of the synthesized nanocomposite for metal ions cleanup from wastewaters. Similar finding was reported by Wu et al. (2015) for desorption of Cd^{2+} from 3D sulfonated reduced graphene oxide adsorbent.

To check the reusability performance of PUF/OB/IO nanocomposite adsorbent, six successive adsorption–desorption cycles have been conducted at the same adsorbent samples and the results are presented in Fig. 10.

The adsorption capacity of PUF/OB/IO nanocomposite adsorbent remains unchanged even after five regeneration cycles. Instead, just a bit increase in the adsorption efficiency was observed after the second cycle. A slight decrease after the fifth cycle indicates that PUF/OB/IO could retain its functionality more than five cycles without significant loss of original adsorptive capacity. These results indicated that spent PUF/OB/IO nanocomposite could be regenerated and further reutilized, which on the other hand supports its practical application as adsorbent.

Application for real samples

Practical application of an adsorbent to real samples is the end goal of adsorption studies for wastewater remediation. Successful application of the studied adsorbents to real samples largely guarantees their effective performance within practical wastewater treatment procedures. For this

Table 3 Comparison between adsorption capacities of different adsorbents for Cd(II)

Adsorbent	pH	Adsorption capacity (mg/g)	References
Bentonite	6.00	3.16	Chen et al. (2011)
Amberlite	4.00	0.640	Kocaoba (2007)
Carbon nanotube	6.00	33.0	Perez-Aguilar et al. (2011)
2-Aminoacetyl thiophenol-modified polyurethane foam	4.00	10.0	Burham (2009)
IDA-chelating resins	5.00	68.6	Wu et al. (2015) and Atia et al. (2008)
PUF/OB/IO nanocomposite	6.00	78.0	This study

Table 4 Characteristic of eluting solutions and percents of Cd^{2+} desorbed

	HCL	HNO_3	H_2SO_4	HNO_3	HNO_3
Concentration (M)	0.100	0.100	0.100	0.500	1.00
Volume (mL)	10.0	10.0	10.0	25.0	25.0
% Cd(II) desorbed	0.500%	10.0%	0.300%	78.0%	99.8%

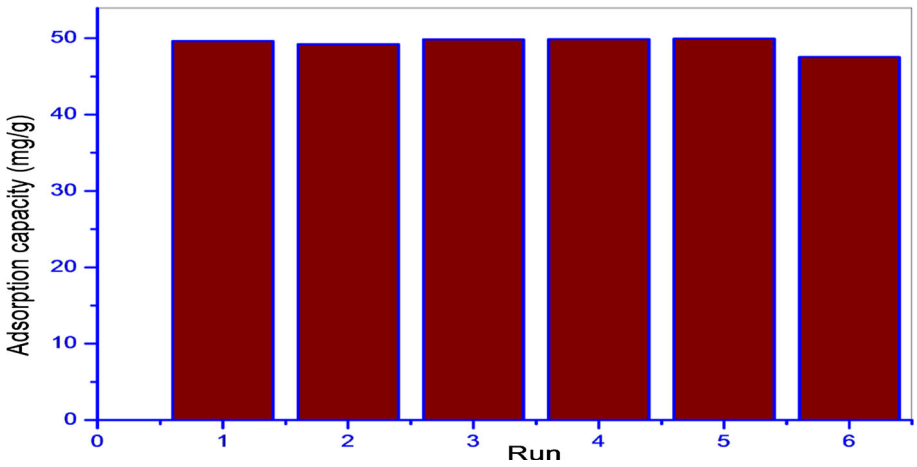

Fig. 10 Adorption cycles of PUF/OB/IO nanocomposite adsorbent for Cd(II) at given experimental condition (pH = 6, metal ion concentration = 100 mg/L and contact time = 60 min)

Table 5 Addition–recovery tests in the experiments for Cd(II) and Zn(II) in different real samples (mean ± SD, $n = 3$)

Sample	Cd^{2+} added (μg/L)	Found (μg/L)	Recovery %
Qaroun Lake water	0.0000	41.00 ± .0001	
	50.00	87.00 ± .0001	95.60
	200.0	233.0 ± .0003	96.70
Bahr Yussef water	0.000	18.00 ± .0001	
	50.00	67.00 ± .0000	98.50
	200.0	213.0 ± .0001	97.70

purpose, two natural water samples are spiked with different amount of Cd^{2+} and mixed together with PUF/OB/IO adsorbent. Recovery of metal ions from the nanocomposite was done using 25 mL 1 M nitric acid. Results of the nanocomposite application for real samples are depicted in Table 5.

All the recovery values for cadmium(II) were in the range of 95.6–98.5%. These values show that the synthesized nanocomposite could be used as a solid-phase extraction material for the preconcentration of cadmium from real samples which strongly recommends the practical application of the synthesized nanocomposite as alternative in the wastewater treatment field.

Conclusion

A novel PUF/OB/IO magnetic nanocomposite adsorbent has been successfully prepared via in situ polymerization technique using 5 wt% OB/IO. The characterization results demonstrated that the organoclay was exfoliated and/or intercalated through the PUF polymer matrix indicating nanostructure formation. The adsorption experiments revealed that the prepared nanocomposite afforded an effective removal of cadmium ions from aqueous media over a wide pH range and within short time. The kinetic study results also showed that the removal of cadmium onto the nanocomposite followed the pseudo-second-order kinetic model with intraparticle and film diffusion steps controls the adsorption rate. Moreover, PUF/OB/IO nanocomposite showed an excellent regeneration feature and excellent applicability for extraction of cadmium ions from natural water samples. The prepared nanocomposite can be considered as an inexpensive, readily available, easily prepared and easily separable adsorbent. These whole aspects strongly suggest that the obtained nanocomposite has a promising potential as an efficient adsorbent for the wastewater treatment discipline.

Acknowledgements The authors would like to declare that this work was conducted at the inorganic chemistry laboratory, Faculty of Science, Fayoum University, Fayoum, Egypt and they didn't receive any specific grant from funding agencies in the public, commercial, or not for profit sectors.

References

Agha MA, Ferrell RE, Hart GF, El Ghar MSA, Abdel-Motelib A (2015) Physical properties and Na-activation of Egyptian bentonitic clays for appraisal of industrial applications. Appl Clay Sci 131:74–83

Atia AA, Donia AM, Elwakeel KZ (2005) Adsorption behaviour of non-transition metal ions on a synthetic chelating resin bearing iminoacetate functions. Sep Purif Technol 43:43–48

Atia AA, Donia AM, Yousif AM (2008) Removal of some hazardous heavy metals from aqueous solution using magnetic chelating resin with iminodiacetate functionality. Sep Purif Technol 61:348–357

Azeem SA, Arafa W, El-Shahat M (2010) Synthesis and application of alizarin complexone functionalized polyurethane foam: pre-concentration/separation of metal ions from tap water and human urine. J Hazard Mater 182:286–294

Bailey SE, Olin TJ, Bricka RM, Adrian DD (1999) A review of potentially low-cost sorbents for heavy metals. Water Res 33:2469–2479

Bergaya F, Lagaly G (2007) Clay mineral properties responsible for CPN performance. CMS workshop lectures. Clay Minerals Society, Chantilly, p 61

Block KA, Trusiak A, Katz A, Alimova A, Wei H, Gottlieb P, Steiner JC (2015) Exfoliation and intercalation of montmorillonite by small peptides. Appl Clay Sci 107:173–181

Burham N (2009) Separation and preconcentration system for lead and cadmium determination in natural samples using 2-aminoacetylthiophenol modified polyurethane foam. Desalination 249:1199–1205

Burham N, Sayed M (2016) Adsorption behavior of Cd^{2+} and Zn^{2+}onto natural egyptian bentonitic clay. Minerals 6:129

Chen Y-G, Ye W-M, Yang X-M, Deng F-Y, He Y (2011) Effect of contact time, pH, and ionic strength on Cd(II) adsorption from aqueous solution onto bentonite from Gaomiaozi, China. Environ Earth Sci 64:329–336

Cottet L, Almeida C, Naidek N, Viante M, Lopes M, Debacher N (2014) Adsorption characteristics of montmorillonite clay modified with iron oxide with respect to methylene blue in aqueous media. Appl Clay Sci 95:25–31

Dong T, Yang L, Zhu M, Liu Z, Sun X, Yu J, Liu H (2015) Removal of cadmium (II) from wastewater with gas-assisted magnetic separation. Chem Eng J 280:426–432

Foo K, Hameed B (2010) Insights into the modeling of adsorption isotherm systems. Chem Eng J 156:2–10

Galbeiro R, Garcia S, Gaubeur I (2014) A green and efficient procedure for the preconcentration and determination of cadmium, nickel and zinc from freshwater, hemodialysis solutions and tuna fish samples by cloud point extraction and flame atomic absorption spectrometry. J Trace Elem Med Biol 28:160–165

Hebbar RS, Isloor AM, Ananda K, Ismail A (2016) Fabrication of polydopamine functionalized halloysite nanotube/polyetherimide membranes for heavy metal removal. J Mater Chem A 4:764–774

Jović-Jovičić N, Milutinović-Nikolić A, Gržetić I, Jovanović D (2008) Organobentonite as efficient textile dye sorbent. Chem Eng Technol 31:567–574

Karapinar N, Donat R (2009) Adsorption behaviour of Cu^{2+} and Cd^{2+} onto natural bentonite. Desalination 249:123–129

Khairy M, El-Safty SA, Shenashen M (2014) Environmental remediation and monitoring of cadmium. TrAC Trends Anal Chem 62:56–68

Khudyakov IV, Zopf DR, Turro NJ (2009) Polyurethane nanocomposites. Des Monomers Polym 12:279–290

Kocaoba S (2007) Comparison of Amberlite IR 120 and dolomite's performances for removal of heavy metals. J Hazard Mater 147:488–496

Kurko SV, Matović LL (2015) Simultaneous removal of Pb^{2+}, Cu^{2+}, Zn^{2+} and Cd^{2+} from highly acidic solutions using mechanochemically synthesized montmorillonite–kaolinite/TiO2 composite. Appl Clay Sci 103:20–27

Lin X, Burns RC, Lawrance GA (2005) Heavy metals in wastewater: the effect of electrolyte composition on the precipitation of cadmium (II) using lime and magnesia. Water Air Soil Pollut 165:131–152

Liu R, Liu F, Hu C, He Z, Liu H, Qu J (2015) Simultaneous removal of Cd(II) and Sb (V) by Fe–Mn binary oxide: positive effects of Cd(II) on Sb (V) adsorption. J Hazard Mater 300:847–854

Luo X, Lei X, Cai N, Xie X, Xue Y, Yu F (2016) Removal of heavy metal ions from water by magnetic cellulose-based beads with embedded chemically modified magnetite nanoparticles and activated carbon. ACS Sustain Chem Eng 4(7):3960–3969

Ma L, Xi Y, He H, Ayoko GA, Zhu R, Zhu J (2016) Efficiency of Fe–montmorillonite on the removal of rhodamine B and hexavalent chromium from aqueous solution. Appl Clay Sci 120:9–15

Machida M, Fotoohi B, Amamo Y, Ohba T, Kanoh H, Mercier L (2012) Cadmium (II) adsorption using functional mesoporous silica and activated carbon. J Hazard Mater 221:220–227

Mahmud HNME, Huq AO, BINTI YAHYA R (2016) The removal of heavy metal ions from wastewater/aqueous solution using polypyrrole-based adsorbents: a review. RSC Adv 6:14778–14791

Marder L, Bernardes AM, Ferreira JZ (2004) Cadmium electroplating wastewater treatment using a laboratory-scale electrodialysis system. Sep Purif Technol 37:247–255

Oliveira LC, Rios RV, Fabris JD, Sapag K, Garg VK, Lago RM (2003) Clay–iron oxide magnetic composites for the adsorption of contaminants in water. Appl Clay Sci 22:169–177

Perez-Aguilar NV, Diaz-Flores PE, Rangel-Mendez JR (2011) The adsorption kinetics of cadmium by three different types of carbon nanotubes. J Colloid Interface Sci 364:279–287

Qiu H, Lv L, Pan B-C, Zhang Q-J, Zhang W-M, Zhang Q-X (2009) Critical review in adsorption kinetic models. J Zhejiang Univ Sci A 10:716–724

Ranđelović M, Purenović M, Matović B, Zarubica A, Momčilović M, Purenović J (2014) Structural, textural and adsorption characteristics of bentonite-based composite. Microporous Mesoporous Mater 195:67–74

Setshedi KZ, Bhaumik M, Songwane S, Onyango MS, Maity A (2013) Exfoliated polypyrrole-organically modified montmorillonite clay nanocomposite as a potential adsorbent for Cr(VI) removal. Chem Eng J 222:186–197

Shah LA, DA SILVA VALENZUELA MDG, EHSAN AM, DíAZ FRV, KHATTAK NS (2013) Characterization of Pakistani purified bentonite suitable for possible pharmaceutical application. Appl Clay Sci 83:50–55

Wang X, Yang L, Zhang J, Wang C, Li Q (2014) Preparation and characterization of chitosan–poly (vinyl alcohol)/bentonite nanocomposites for adsorption of Hg(II) ions. Chem Eng J 251:404–412

Wu L, Ye Y, Liu F, Tan C, Liu H, Wang S, Wang J, Yi W, Wu W (2013) Organo-bentonite-Fe_3 O_4 poly (sodium acrylate) magnetic superabsorbent nanocomposite: synthesis, characterization, and Thorium (IV) adsorption. Appl Clay Sci 83:405–414

Wu S, Zhang K, Wang X, Jia Y, Sun B, Luo T, Meng F, Jin Z, Lin D, Shen W (2015) Enhanced adsorption of cadmium ions by 3D sulfonated reduced graphene oxide. Chem Eng J 262:1292–1302

Yukselen Y, Kaya A (2008) Suitability of the methylene blue test for surface area, cation exchange capacity and swell potential determination of clayey soils. Eng Geol 102:38–45

Zhao G, Zhang H, Fan Q, Ren X, Li J, Chen Y, Wang X (2010) Sorption of copper (II) onto super-adsorbent of bentonite–polyacrylamide composites. J Hazard Mater 173:661–668

Zhao F, Tang WZ, Zhao D, Meng Y, Yin D, SILLANPää M (2014) Adsorption kinetics, isotherms and mechanisms of Cd(II), Pb(II), Co(II) and Ni(II) by a modified magnetic polyacrylamide microcomposite adsorbent. J Water Process Eng 4:47–57

Zhou L, Li G, An T, Li Y (2010) Synthesis and characterization of novel magnetic Fe_3O_4/polyurethane foam composite applied to the carrier of immobilized microorganisms for wastewater treatment. Res Chem Intermed 36:277–288

Zhu J, He H, Guo J, Yang D, Xie X (2003) Arrangement models of alkylammonium cations in the interlayer of HDTMA + pillared montmorillonites. Chin Sci Bull 48:368–372